Optimal swimming of a sheet

Thomas D. Montenegro-Johnson and Eric Lauga[*]

Department of Applied Mathematics and Theoretical Physics, Centre for Mathematical Sciences, University of Cambridge,
Wilberforce Road, Cambridge CB3 0WA, UK

Propulsion at microscopic scales is often achieved through propagating traveling waves along hairlike organelles called flagella. Taylor's two-dimensional swimming sheet model is frequently used to provide insight into problems of flagellar propulsion. We derive numerically the large-amplitude wave form of the two-dimensional swimming sheet that yields optimum hydrodynamic efficiency: the ratio of the squared swimming speed to the rate-of-working of the sheet against the fluid. Using the boundary element method, we show that the optimal wave form is a front-back symmetric regularized cusp that is 25% more efficient than the optimal sine wave. This optimal two-dimensional shape is smooth, qualitatively different from the kinked form of Lighthill's optimal three-dimensional flagellum, not predicted by small-amplitude theory, and different from the smooth circular-arc-like shape of active elastic filaments.

PACS number(s): 87.17.Jj, 87.85.gj, 87.85.gf

I. INTRODUCTION

The microscopic world is teeming with organisms and cells that must self-propel through their fluid environment in order to survive or carry out their functions [1]. At these very small scales, viscous forces dominate inertia in fluid flows, and a common method of overcoming the challenges of viscous propulsion through the fluid environment is by propagating waves along slender, hairlike organelles called flagella or cilia [2,3]. To examine the fluid mechanical basis for microscopic propulsion, Taylor [4] considered a simplified flagellum model comprising a two-dimensional sheet exhibiting small-amplitude traveling waves. This seminal work subsequently sparked the development of other techniques for examining Newtonian viscous flows such as slender-body theory [5–7] and resistive-force theory [2,8], as well as other models for non-Newtonian swimming based on distribution of force singularities [9,10].

Due to its analytical tractability and agreement with more involved approaches in the small-amplitude limit, Taylor's swimming sheet has been used to give insight into many fundamental problems in microscale propulsion, such as hydrodynamic synchronization between waving flagella [4,11–13], swimming in non-Newtonian fluids [14–16], and swimming past deformable membranes [10]. These approaches are typically characterized by asymptotic expansion of the flagellar wave form under the condition that the amplitude of the waves is small when compared to the wavelength. Recently, Taylor's small-amplitude expansion was formally extended to arbitrarily high order for a pure sine wave, a method able to produce results comparable to full numerical simulations of large-amplitude sine waves with the boundary element method [17].

Motivated by the role of evolutionary pressures on the shape and kinematics of swimming microorganisms, it is relevant to investigate which flagellar wave form is the most energetically efficient for the cell. For an infinite flagellum, Lighthill [2] showed that in the local drag approximation of resistive-force theory, the hydrodynamically-optimal flagellar wave form has a constant tangent angle to the swimming direction. This leads to the shape of a smooth helix in three dimensions, and a singular triangle wave in two dimensions. While the helical wave form is commonly observed in bacterial flagella [18,19], unsurprisingly the kinked planar wave form is not. Spagnolie and Lauga [20] showed that this shape singularity in Lighthill's flagellum can be regularized by penalizing the swimming efficiency by the elastic energy required to bend a flagellum, which might provide one explanation for its absence in nature. This model was then improved upon by Lauga and Eloy [21] by proposing an energetic measure based on the internal molecular cost necessary to deform the active flagellum. For finite-length flagella, Pironneau and Katz [22] showed that traveling waves are fundamental to optimal propulsion. Using resistive force theory, they then analyzed optimal patterns for model spermatozoa exhibiting small-amplitude planar sinusoidal waves and finite-amplitude triangle waves. The optimal stroke pattern of Purcell's finite three-link swimmer was found by Tam and Hosoi [23], who then went on to consider optimal gaits for the green alga *Chlamydomonas* [24].

While all past optimization work has focused on three-dimensional slender filaments, the optimal wave form of Taylor's two-dimensional swimming sheet has yet to be considered. Although the two-dimensionality of the problem makes it less realistic as a model for swimming cells, the fluid dynamics around a sheet can be computed very accurately, allowing us to bypass various hydrodynamic modeling approximations employed in three dimensions. In the present study, we use the boundary element method to examine a sheet propagating large-amplitude waves of arbitrary shape. We derive computationally the wave form leading to swimming with maximum hydrodynamic efficiency. We show that the optimal wave form for the swimming sheet is a regularized cusp wave not predicted by small-amplitude analysis. The optimal is qualitatively different from three-dimensional swimmers, both the kinked triangle of Lighthill's hydrodynamically-optimal flagellum [2] and the circular arcs of internally-optimal active filaments [21], and indicates a qualitative difference between two- and three-dimensional swimming at large amplitude.
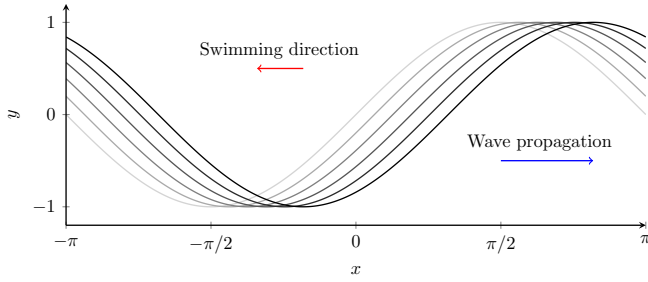
*e.lauga@damtp.cam.ac.uk

FIG. 1. (Color online) A schematic of the wave propagation of a swimming sheet, here illustrated by a single sine-wave mode, showing the computational domain ($-\pi$ to π along the x axis), direction of wave propagation (in the swimming frame), and direction of swimming.

II. FORMULATION OF THE PROBLEM

Newtonian fluid mechanics at microscopic scales is governed by the incompressible Stokes flow equations,

$$\mu \nabla^2 \mathbf{u} = \nabla p, \quad \nabla \cdot \mathbf{u} = 0, \tag{1}$$

where $\mathbf{u}$ is the fluid velocity field, p the dynamic pressure, and μ is the dynamic viscosity, hereafter nondimensionalized to $\mu = 1$.

We consider the waving sheet model illustrated in Fig. 1, and assume the wave form to be fixed and to travel along the positive x direction at unit speed. The infinite sheet is periodic over the interval $[-\pi, \pi]$, and swimming is expected to occur in the $-x$ direction, opposite to the direction of propagation of the wave [4]. Since the sheet is infinite, there is no extrinsic length scale to the problem, and as such we hereafter nondimensionalize lengths using the reciprocal of the wave number, k^{-1}. In order for net swimming to take place with no rotation, we require the wave to be odd about the axis $x = 0$, i.e., ask that $y([0, -\pi], t) = -y([0, \pi], t)$. Without loss of generality, the wave form may therefore be described as a Fourier-sine series where the shape in the swimming frame is described by $y(x, t)$ with

$$y(x, t) = \sum_{p=1}^{P} B_p \sin[p(x - t)]. \tag{2}$$

Even modes for the shape, B_{2q} with q any integer, are always obtained by our optimization algorithm to be zero, indicating that optimal wave forms are front-back symmetric waves. The physical reason underlying this front-back symmetry is unclear. Due to kinematic reversibility, if the shape was asymmetric then an equally optimal wave form would be its front-back mirror image, and thus the optimization procedure would always lead to two symmetric solutions. This is not the case and a unique, front-back symmetric shape is always obtained. We thus consider a general wave form represented by

$$y(x, t) = \sum_{n=1}^{N} B_n \sin[(2n - 1)(x - t)], \tag{3}$$

and use our computational approach to derive the optimal series of coefficients $\{B_n\}_N, n \leqslant N$ for increasing N. The lack of an extrinsic length scale to the infinite sheet means that our choice of first mode is in some sense arbitrary, and thus we

will consider solutions for which $|B_1| > 0$, in order to define a fundamental period to the wave.

To derive the hydrodynamically-optimal wave form we use the standard definition of swimming efficiency introduced by Lighthill [2]. We therefore compare a useful rate of swimming, $\sim U^2$, to the rate of working of the sheet against the fluid, $W = -\int_S \mathbf{u} \cdot \boldsymbol{\sigma} \cdot \mathbf{n} \, ds$, where the fluid stress is $\boldsymbol{\sigma} = -p\mathbf{I} + [\nabla \mathbf{u} + (\nabla \mathbf{u})^T]$, S is the surface of the swimmer over one wavelength, and $\mathbf{n}$ is the unit normal to the sheet into the fluid. We thus seek the set of coefficients $\{B_n\}_N$ that maximize the hydrodynamic efficiency, $\mathcal{E}$, defined as

$$\mathcal{E} = \frac{U^2}{-\int_S \mathbf{u} \cdot \boldsymbol{\sigma} \cdot \mathbf{n} \, ds}, \tag{4}$$

and numerically compute the value of the swimming speed, U, and surface stress, $\boldsymbol{\sigma} \cdot \mathbf{n}$.

In order to impose velocity conditions on the surface of the sheet, we solve the problem in a frame of reference that moves with the propagating wave. Since the sheet is stationary in this frame, the velocity of material elements is purely tangential [2]. By subtracting the normalized wave speed, this allows us to retrieve the boundary conditions everywhere along the sheet as

$$u(\mathbf{x}) = -Q \cos \theta(\mathbf{x}) + 1, \quad v = -Q \sin \theta(\mathbf{x}), \tag{5}$$

where Q denotes the ratio between the arclength of the wave form in one wavelength to the wavelength measured along the x direction and $\theta(\mathbf{x})$ is the tangent angle of the sheet measured about the x axis. Both the value of Q and the distribution of θ are functions of the wave geometry only, and thus of the coefficients $\{B_n\}_N$.

III. COMPUTATIONAL APPROACH

In order to compute the flow field generated by the sheet, and the resultant surface stresses, we employ the boundary element method [25] with two-dimensional, periodic Green's functions as in Pozrikidis [26] and Sauzade *et al.* [17]. At any point $\mathbf{x}$ along the sheet, the velocity at that point is given by the surface integral

$$u_j(\mathbf{x}) = \frac{1}{2\pi} \int_S [S_{ij}(\mathbf{x} - \mathbf{x}') f_i(\mathbf{x}') - T_{ijk}(\mathbf{x} - \mathbf{x}') u_i(\mathbf{x}') n_k(\mathbf{x}')] ds(\mathbf{x}'), \tag{6}$$

where $\mathbf{n}(\mathbf{x}')$ is the unit normal pointing into the fluid at $\mathbf{x}'$ and $f_i = \sigma_{ij} n_j$. Using the notation $r = |\hat{\mathbf{x}}|$, the stokeslet tensor, S_{ij}, and stresslet, T_{ijk}, are given by

$$S_{ij}(\hat{\mathbf{x}}) = \delta_{ij} \ln r - \frac{\hat{x}_i \hat{x}_j}{r^2}, \quad T_{ijk}(\hat{\mathbf{x}}) = 4 \frac{\hat{x}_i \hat{x}_j \hat{x}_k}{r^4}, \tag{7}$$

and represent the solution to Stokes flow due to a point force in two dimensions and the corresponding stress respectively. Since we are modeling an infinite, 2π-periodic sheet, we have velocity contributions at $\mathbf{x}$ from an infinite sum of stokeslets and stresslets,

$$\mathbf{S}^p = \sum_{n=-\infty}^{\infty} \mathbf{I} \ln r_n - \frac{\hat{\mathbf{x}}_n \hat{\mathbf{x}}_n}{r_n^2}, \quad \mathbf{T}^p = \sum_{n=-\infty}^{\infty} 4 \frac{\hat{\mathbf{x}}_n \hat{\mathbf{x}}_n \hat{\mathbf{x}}_n}{r_n^4}, \tag{8}$$

where $\hat{\mathbf{x}}_n = (x - x' + 2\pi n, y - y')$ for singularities positioned at $\mathbf{x}'$. These infinite sums may be conveniently expressed in a closed form as

$$
\begin{aligned}
S_{xx}^p &= A + \hat{y}\partial_{\hat{y}}A - 1, & T_{xxy}^p &= 2\partial_{\hat{y}}(\hat{y}\partial_{\hat{y}}A), \\
S_{yy}^p &= A - \hat{y}\partial_{\hat{y}}A, & T_{xyy}^p &= -2\hat{y}\partial_{\hat{x}\hat{y}}A, \\
S_{xy}^p &= -\hat{y}\partial_{\hat{x}}A = S_{yx}^p, & T_{yyy}^p &= 2(\partial_{\hat{y}}A - \hat{y}\partial_{\hat{y}\hat{y}}A), \\
T_{xxx}^p &= 2\partial_{\hat{x}}(2A + \hat{y}\partial_{\hat{y}}A), & T_{ijk}^p &= T_{kij}^p = T_{jki}^p,
\end{aligned}
\tag{9}
$$

where $A = \frac{1}{2}\ln[2\cosh(\hat{y}_0) - 2\cos(\hat{x}_0)]$. Note that these are equivalent to, but differ by a minus sign from, those found in Sauzade *et al.* [17], due to our adoption of the sign convention from Pozrikidis [26].

For the computational procedure, the sheet is discretized into 500 straight line segments of constant force per unit length; i.e., the components $f_{1,2}$ in Eq. (6) are constant over each straight line element. This discretization breaks Eq. (6) into a sum of line integrals of singularities, multiplied by the unknown force per unit length. Numerical evaluation of each nonsingular line integral is performed with four-point Gaussian quadrature, while singular integrals are treated analytically. This numerical discretization produced a $<0.02\%$ relative difference in the calculated swimming velocity and efficiency for both kinked and unkinked example sheets when compared to simulations with 600 and 800 elements with 8- and 16-point Gaussian quadrature, while still allowing calculation in a reasonable time. By decoupling the numerical quadrature from the force discretization, comparable accuracy is achieved for relatively smaller linear systems [27]. The computational mesh is refined locally around regions of high curvature appearing as a result of the optimization in order to resolve potential kinks and singular shapes. Using these parameters, we find convergence of the wave form and optimal efficiency for $N = 30$. In order to reach this number of coefficients quickly, it is important to provide a good starting guess for the coefficients B_n at the beginning of the optimization procedure. Since we are interested in the convergence of our wave form with an increased number of points, we numerically optimize for $n = 1, \ldots, 30$ sequentially, and use the converged optimal coefficients for the $n = N - 1$ wave form as an initial guess for the $n = N$ wave form, with B_N initially set to zero. In order to ensure that our solution represents the global maximum of the hydrodynamic efficiency (4), multiple initial conditions were tried, all found to be optimized to the same wave form. Optimization is carried out using the standard "fminunc" function in MATLAB employing the "quasi-Newton" algorithm.

IV. THE SHAPE OF THE OPTIMAL SWIMMING SHEET

With this framework established, we are able to compute the shape of the optimal swimming sheet. It is first instructive to ask what would be predicted from the analytical small-amplitude approach. In that case, the wave form is written as

$$
y(x,t) = \epsilon \sum_{n=1}^{\infty} B_n e^{in(x-t)},
\tag{10}
$$

where ϵ is a small dimensionless amplitude. To second order in the amplitude [4], the swimming speed, U, and work done

against the fluid, W, are given by

$$
U \sim \sum_{n=1}^{\infty} n^2 |B_n|^2 \epsilon^2, \quad W \sim \sum_{n=1}^{\infty} n^3 |B_n|^2 \epsilon^2.
\tag{11}
$$

Because the work done is proportional to n^3, whereas the swimming velocity is proportional to n^2, higher-order modes are energetically penalized compared to lower modes. Therefore for a fixed amount of mechanical power expended by the swimmer, it is more efficient to distribute all of that power to the first mode $n = 1$; under the small-amplitude approximation, the most efficient wave form is therefore a single sine wave of period 2π.

Relaxing the small-amplitude constraint, we show in Fig. 2(a) the optimal wave form obtained numerically for $N = 30$ odd Fourier modes. The set of coefficients B_n that describe this wave form are given in the Appendix and a three-dimensional sheet propagating this wave is further shown in Fig. 2(b). The optimal swimming sheet appears to take the shape of a regularized cusp wave, qualitatively different from the single-mode sine wave predicted by the asymptotic analysis. We further plot in Fig. 2(c) the distribution of slopes along the sheet, showing that the wave has an almost straight section (constant slope), steepening towards smooth wave crest. The angle of the slope at the point of symmetry $x = 0$ is approximately $36.1°$, close to the optimum value of $40.06°$ obtained for Lighthill's three-dimensional flagellum via resistive-force theory with a drag anisotropy ratio of $1/2$ [2]. We display in Fig. 2(d) the distribution of curvature along the sheet; while the curvature at the wave crest increases, it remains finite. For comparison, our predicted optimal wave form is plotted against the pure sine wave of small-amplitude theory [4] and the triangle wave predicted by Lighthill [2] in Fig. 2(e).

Since our optimization procedure finds the optimal solution for incremental values of the number of coefficients, N, used to describe the wave, we can investigate convergence of all optimal wave forms described by N ranging from 1 to 30. The convergence for the swimming efficiency is shown in Fig. 3(a) while the dependence of the maximum curvature on N is plotted in Fig. 3(b). For $N = 30$, the optimal wave form is over 25% more efficient than the optimal one-mode sine wave ($N = 1$). The swimming efficiency appears to reach its asymptote near $N = 13$, which corresponds to the peak in the maximum curvature, but thereafter continues to increase slightly before reaching its converged value of $\mathcal{E} \approx 0.11065$. This slight increase is accompanied by a decrease in the maximum curvature of the optimal wave forms for $N \geqslant 14$. Up to $N = 13$, it appears that subsequent modes serve to steepen the wave form as it approaches around the crest. Such steepening is likely hydrodynamically favorable in two dimensions since fluid cannot pass around the sheet as it would around three-dimensional flagella. However, steepening results in a region of high curvature at the wave crest, which induces locally high viscous dissipation in the fluid, and so there appears to be an efficiency trade-off between wave steepening and minimizing curvature. For $N \geqslant 14$, the wavelength of the Fourier modes is on the order of the length of the cap on the wave crest. These modes are then able to decrease the maximum curvature without decreasing the
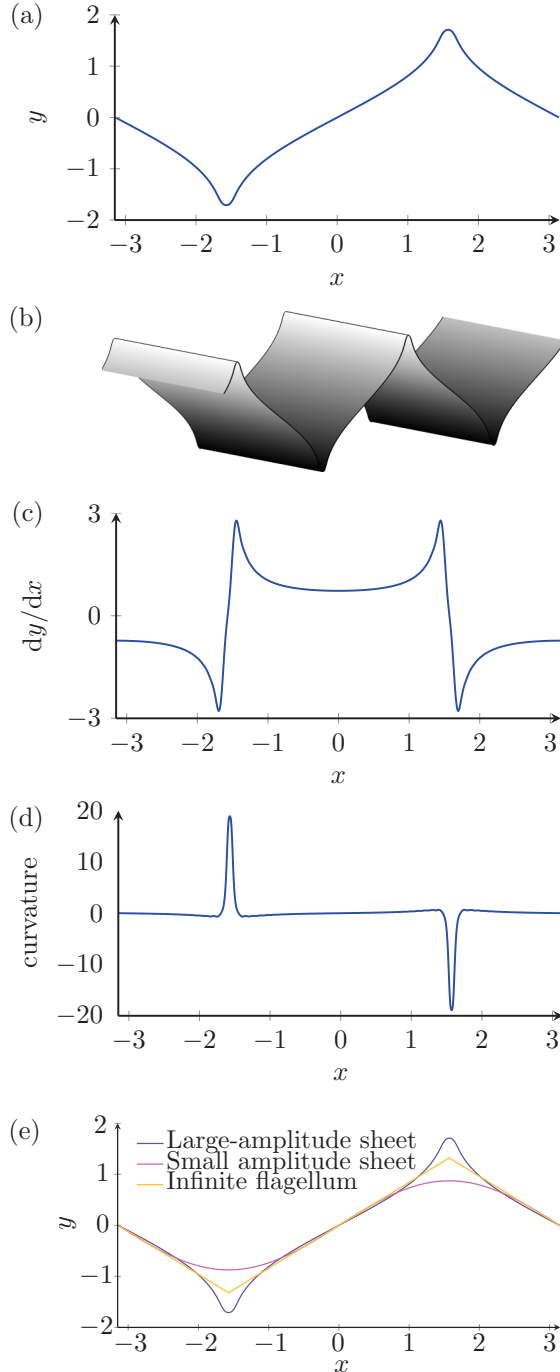
(a)

(b)

(c)

(d)

(e)

FIG. 2. (Color online) The optimal swimming sheet. (a) Optimal wave form obtained computationally, which exhibits an almost straight region followed by a steepening of the wave crest into a rounded cap. (b) Three-dimensional visualization of the optimal swimming sheet. Distribution of slope (c) and curvature (d) of the optimal wave form showing largely straight regions. (e) Wave form of the optimal sheet shown for comparison with the pure sine wave predicted by small amplitude theory [4] and Lighthill's optimal triangle wave for a flagellum with drag anisotropy ratio of 1/2 [2].

slope of the wave, yielding small increases in efficiency until the curvature converges for $N \geqslant 30$. We further display the convergence of the optimal wave form as a function of the number of coefficients, N, in Fig. 4. Despite the decrease in
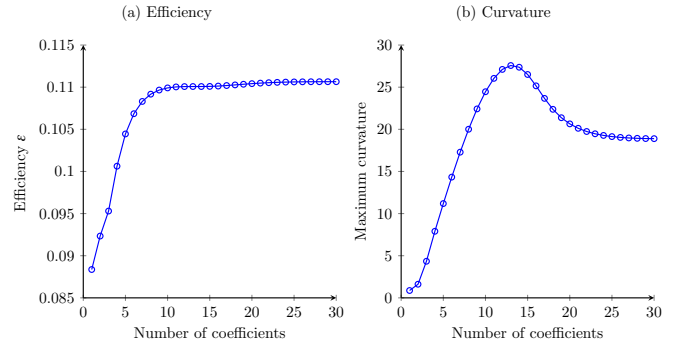

FIG. 3. (Color online) Convergence of the swimming efficiency (a) and maximum wave curvature (b) as a function of the number of odd Fourier modes in the optimization, N.

maximum curvature seen in Fig. 3(b) for $N \geqslant 14$, all wave forms between $N = 10$ and 30 are virtually indistinguishable by eye.

The trade-off between wave steepening and reducing curvature can be further investigated by examining a family of waves of the form

$$B_n = C \frac{(-1)^{n-1}}{(2n-1)^m}, \quad n \geqslant 1, \tag{12}$$

where C is a constant. The value of m dictates the decay of the Fourier coefficients with the Fourier mode, and with the choice $m = 2$, Eq. (12) leads to the triangular wave form of Lighthill's optimal flagellum. The choice of alternating sign is informed both by the series for the triangle wave, and by the coefficients of our optimal solution (up to $N = 14$). Cusps are obtained for $m < 2$ and rounded-off waves for $m > 2$ and, by truncating the series at small values of N, we retrieve an approximate regularized cusp wave. Figure 5 shows isocontours of the efficiency of waves described by Eq. (12) for the optimal value of the amplitude, C, as a function of the number of coefficients used to describe the wave, N, and the decay rate, m. The optimal efficiency $\mathcal{E} = 0.1037$ of such waves occurs when $N = 9$, for $C = 1.237$ and $m = 1.609$, which corresponds to a slower decay of the Fourier modes than Lighthill's wave. The wave form associated with this optimal is plotted inset in Fig. 5 (blue, solid), showing a strong similarity to our fully converged optimal computed for 30 coefficients (black, dashed).
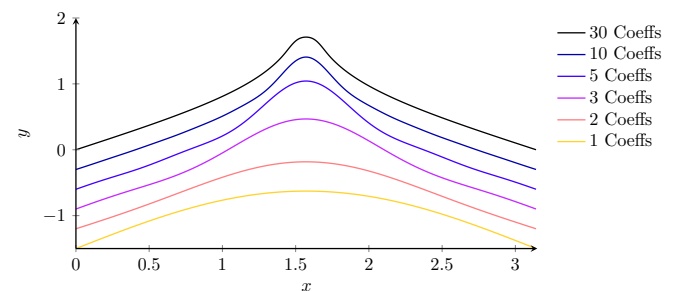

FIG. 4. (Color online) Convergence of the shape of the optimal wave form for increasing numbers of odd coefficients. Shapes are shifted by 0.1π along the y direction for visualization.
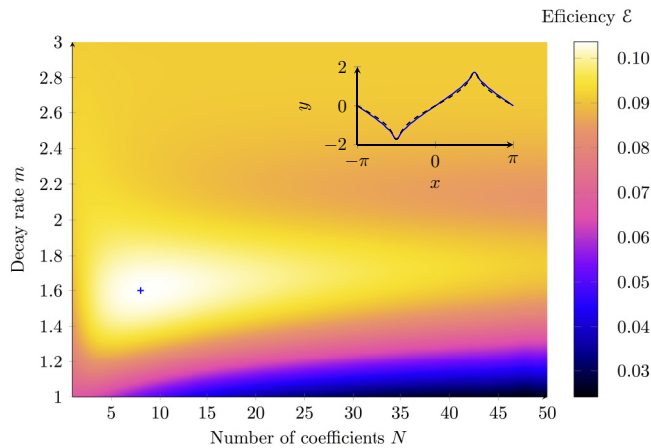
FIG. 5. (Color online) Efficiences of optimal truncated "cusp-like" wave forms (12) as a function of number of odd modes in the description N and decay rate m, showing a maximum at $N = 9, m \approx 1.6$ for regularized cusps. The wave form corresponding to this maximum is shown inset (blue, solid) in comparison to the full optimal of Fig. 2(a) (black, dashed), showing good qualitative agreement.

If a large enough number of odd modes ($N \geqslant 50$) is used to describe the curve, the kink at the wave crest is sufficiently resolved as to no longer be regularized. In this case, the optimal jumps to an unkinked profile with which $C = 0.9173$ and $m = 2.923$, yielding an efficiency of just 0.0912 and demonstrating the detrimental effect of kinked wave forms on hydrodynamic efficiency when nonlocal effects are taken into account. The optimal within this family is thus more efficient than any kinked wave. Furthermore, this result suggests that by

fully resolving the hydrodynamics around Lighthill's optimal flagellum, viscous dissipation associated with the kink might also regularize this wave form.

V. DISCUSSION

Taylor's swimming sheet model is commonly used to address a range of phenomena in the biological physics of small-scale locomotion. A natural question to raise is the relevance of a two-dimensional geometry to the three-dimensional locomotion of flagellated cells. In this Rapid Communication, we used the boundary element method to compute the swimming efficiency of arbitrary wave forms in two dimensions. By focusing on the question of optimal wave form for locomotion, we show that the optimal two-dimensional wave form is a regularized cusp, which is about 25% more efficient than a simple sine wave. This result is different from the three-dimensional hydrodynamically-optimal triangle wave derived by Lighthill [2]; the slope of the straight section is shallower, the wave form steepens towards the wave crest, and there is no discontinuity in the slope but rather a regularized cusp. The result is also different from the three-dimensional internally-optimal wave, which is composed of circular arcs joined by straight lines [21]. Although it is known that the dynamics of a swimming sheet can provide qualitative insight into the hydrodynamics of small-scale locomotion, differences with three-dimensional results exist therefore at large amplitude.

APPENDIX: COEFFICIENTS OF THE OPTIMAL WAVE FORM

The Fourier coefficients for the optimal wave form for $N = 30$ are given as follows:

$B_1 = 1.146$	$B_2 = -0.2494$	$B_3 = 0.1205$	$B_4 = -0.07090$	$B_5 = 0.04534$
$B_6 = -0.03017$	$B_7 = 0.02039$	$B_8 = -0.01378$	$B_9 = 0.009180$	$B_{10} = -0.005925$
$B_{11} = 0.003611$	$B_{12} = -0.001973$	$B_{13} = 0.0008291$	$B_{14} = -5.110 \times 10^{-5}$	$B_{15} = -0.0004558$
$B_{16} = 0.0007617$	$B_{17} = -0.0009207$	$B_{18} = 0.0009738$	$B_{19} = -0.0009531$	$B_{20} = 0.0008831$
$B_{21} = -0.0007831$	$B_{22} = 0.0006675$	$B_{23} = -0.0005475$	$B_{24} = 0.0004310$	$B_{25} = -0.0003239$
$B_{26} = 0.0002299$	$B_{27} = -0.0001515$	$B_{28} = 8.958 \times 10^{-5}$	$B_{29} = -4.427 \times 10^{-5}$	$B_{30} = 1.472 \times 10^{-5}$

[1] D. Bray, *Cell Movements* (Garland Publishing, New York, 2000).

[2] J. Lighthill, *Mathematical Biofluiddynamics* (SIAM, Philadelphia, PA, 1975).

[3] S. Childress, *Mechanics of Swimming and Flying* (Cambridge University Press, Cambridge, UK, 1981).

[4] G. I. Taylor, Proc. R. Soc. London A **209**, 447 (1951).

[5] G. J. Hancock, Proc. R. Soc. London A **217**, 96 (1953).

[6] J. B. Keller and S. I. Rubinow, J. Fluid Mech. **75**, 705 (1976).

[7] R. E. Johnson, J. Fluid Mech. **99**, 411 (1980).

[8] J. Gray and G. J. Hancock, J. Exp. Biol. **32**, 802 (1955).

[9] T. D. Montenegro-Johnson, A. A. Smith, D. J. Smith, D. Loghin, and J. R. Blake, Euro. Phys. J. E **35**, 1 (2012).

[10] J. C. Chrispell, L. J. Fauci, and M. Shelley, Phys. Fluids **25**, 013103 (2013).

[11] G. J. Elfring and E. Lauga, Phys. Rev. Lett. **103**, 088101 (2009).

[12] G. J. Elfring, O. S. Pak, and E. Lauga, J. Fluid Mech. **646**, 505 (2010).

[13] G. J. Elfring and E. Lauga, J. Fluid Mech. **674**, 163 (2011).

[14] E. Lauga, Phys. Fluids **19**, 083104 (2007).

[15] J. Teran, L. Fauci, and M. Shelley, Phys. Rev. Lett. **104**, 038101 (2010).

[16] T. D. Montenegro-Johnson, D. J. Smith, and D. Loghin, Phys. Fluids **25**, 081903 (2013).

[17] M. Sauzade, G. J. Elfring, and E. Lauga, Physica D **240**, 1567 (2011).

[18] C. Brennen and H. Winet, Annu. Rev. Fluid Mech. **9**, 339 (1977).

[19] S. E. Spagnolie and E. Lauga, Phys. Rev. Lett. **106**, 058103 (2011).

[20] S. E. Spagnolie and E. Lauga, Phys. Fluids **22**, 031901 (2010).

[21] E. Lauga and C. Eloy, J. Fluid Mech. **730**, R1 (2013).

[22] O. Pironneau and D. F. Katz, J. Fluid Mech. **66**, 391 (1974).

[23] D. Tam and A. E. Hosoi, Phys. Rev. Lett. **98**, 068105 (2007).

[24] D. Tam and A. E. Hosoi, Proc. Natl. Acad. Sci. USA **108**, 1001 (2011).

[25] G. K. Youngren and A. Acrivos, J. Fluid Mech. **69**, 377 (1975).

[26] C. Pozrikidis, J. Fluid Mech. **180**, 495 (1987).

[27] D. J. Smith, Proc. R. Soc. A **465**, 3605 (2009).